Cyclic Cluster Growth in Ferroelectric Perovskites

Doru C. Lupascu
Institute of Materials Science, Darmstadt University of Technology, Petersenstrasse 23, 64287 Darmstadt, Germany

Ute Rabe
Fraunhofer Institute for Non-Destructive Testing, Building 37, University, 66123 Saarbrücken, Germany
(Received 23 April 2002; published 11 October 2002)

We prove that point defect clustering in perovskite ferroelectrics and the subsequent loss in switchable polarization can occur only if the depolarizing fields are locally unscreened during certain fractions of time in each of the multiple bipolar electric field cycles.

DOI: 10.1103/PhysRevLett.89.187601 PACS numbers: 77.22.Ej, 68.37.Ps, 77.80.Dj, 77.84.Dy

The loss in amplitude of the ferroelectric polarization hysteresis by cyclic external electrical loading has been a puzzling process limiting the use particularly of polycrystalline ferroelectrics in large consumer markets [1,2]. In polycrystalline perovskite ferroelectrics domain wall motion is the dominant switching mechanism of polarization reorientation [3], because sufficient numbers of domains already exist [4,5] and no nucleation is needed. The domain wall mobility in turn is determined by the interaction with structural imperfections such as the outer perimeter of a crystal, grain boundaries, inclusions, or point defects and their clusters [6]. While a homogeneous distribution of point defects in the bulk of a crystal yields only a slightly reduced domain wall velocity [6], larger clusters may completely block the motion of certain domain walls [7]. Three microphysical aspects essential for the cyclic fatigue induced reduction of switchable polarization are presented here: The formation of charged planar defect clusters within the bulk grains, the necessity of unscreened depolarizing fields for cluster growth, and a simple rate model expressing the cluster growth as a function of cycle number. Together they yield a unified picture of point defect clustering under bipolar electric fields.

In perovskite-type structures, point defects and especially oxygen vacancies may form ordered substructures in the lattice [8], particularly when tempered under highly reducing conditions [9]. In order to compensate the spontaneous polarization of a ferroelectric, unit cells in the immediate neighborhood of a defect ion reorient to reduce the energy of the charged defect. A head-to-head orientation of the polarization sharing the axial orientation of the surrounding domain is a necessary theoretical consequence (equivalently tail-to-tail) [10]. As the spontaneous polarization in lead-zirconate-titanate amount to approximately half an elementary charge per unit cell, one elementary charge can fully be compensated by a head-to-head structure. Such antiparallel domain structures around point defects stabilize further defects of the same polarity in order to reduce the total energy of the system [11]. Microdomains were proposed to occur around isolated Ta^{3+}-oxygen vacancy ($V_O^{\bullet\bullet}$) defect pairs as reflected in modified luminescence spectra in $KTaO_3$ [12]. Scott and Dawber then recently proposed that oxygen vacancies will form ordered substructures as a result of bipolar fatigue analogous to the ones formed under highly reducing conditions [13,14]. Ordered substructures of oxygen vacancies were also found to be forming at the interface to external electrodes [15], which was also proposed to yield the necessary pinning force for the fatigue effect in thin films. Furthermore, the same authors proposed an oxygen vacancy migration model explaining the fatigue effect [16]. Thus far, an experimental proof of such clusters due to fatigue is missing.

A necessary consequence of the head-to-head structure around point defects is the formation of needle domains [12]. These are geometrically identical to domains nucleating during switching [6]. Figure 1 illustrates the general structure of such needle domains induced by a planar cluster and different possibilities of interaction with 180° and 90° domain walls. Similar images can be drawn for 90° domain needles not changing the underlying physics.

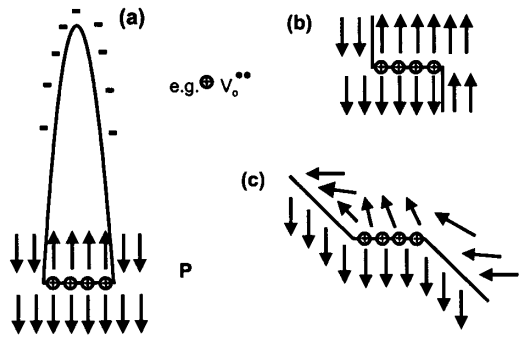

FIG. 1. (a) Needle domain at a point defect cluster (⊕) in a significantly larger surrounding domain. The needle tip is a charged domain wall. (b) 180° and (c) 90° domain wall intersecting with a point defect cluster. While the 180° domain wall is stably located at the cluster, the 90° domain wall stores a significant amount of potential energy. In each case, the cluster hinders domain wall motion.

Polycrystalline soft tetragonal lead-zirconate-titanate $\{Pb_{0.99}[Zr_{0.45}Ti_{0.47}(Ni_{0.33}Sb_{0.67})_{0.08}]O_3$, PZT$\}$ close to the morphotropic phase boundary was contacted by fired silver electrodes and cycled for 10^8 bipolar cycles at 50 Hz [17] and 2 kV/mm, around twice the coercive field. After cycling, the ferroelectric hysteresis loop (at 20 mHz) dropped to about 30% of its initial amplitude in polarization. Simultaneously, the total energy of acoustic emissions emanating from the sample increased by an order of magnitude expressing the increased interaction of extended defects with the domain system [17]. After polishing and intensive chemical etching, the surfaces of these samples exhibited particular etch grooves which were distinctly different from grain boundaries and domains and not found in virgin samples. The sizes of the straight but partly feathery etch grooves ranged from fractions up to the full grain size (average 5 μm). Thus far, it has been unclear whether the origins of these etch grooves were microcracks or actually the suggested images of clusters of charged point defects causing a reduced or completely lost domain wall mobility [17].

Figure 2 displays atomic force microscopic (AFM) images of the domain structure before and after fatigue on a nonetched surface. In piezoelectric mode, a sinusoidal voltage is applied between the sample and a sensor tip coated with a conducting layer serving as a miniaturized electrode of several nm diameter [18,19]. The frequency of the ac voltage was close to the first contact resonance of the cantilever [20]. This technique enhances the response to local variations of piezoelectric polarization due to resonance amplification yielding sharp images of the different polarization projections onto the surface. As the excited sample surface region here is smaller than the domains [21], true domain images can be obtained.

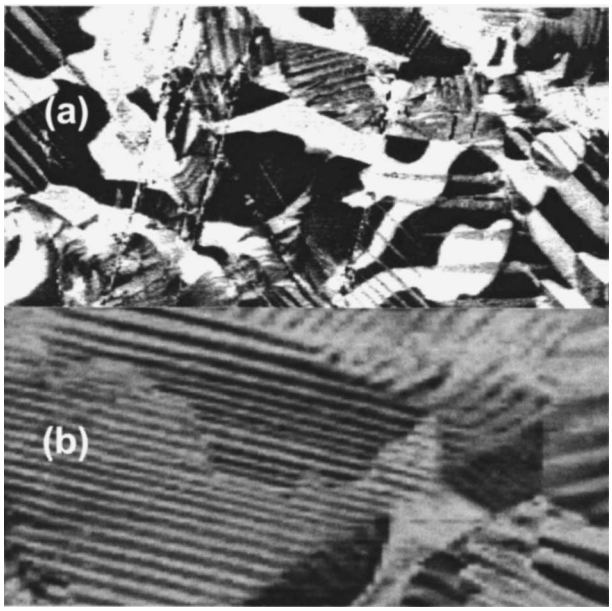

FIG. 2. Atomic force microscopic images of domain structures (a) before and (b) after cycling (image width 10 μm).

Before cycling, the domain structure consists of mostly watermark patterns of rounded contours of 180° domain walls [Fig. 2(a)]. After cycling, it is almost completely replaced by needle domains emanating from the grain boundaries or from planar structures within the grains [Fig. 2(b)]. In some grains, chessboard 180° domain patterns are found for the intersecting domains known, e.g., from $BaTiO_3$ [22].

Figure 3 displays an AFM image of the domain structure encountered around clusters in PZT after fatigue. The arrows indicate locations of clusters in the interior of a grain and the dashed lines the grain boundaries. These structures are not simply 180° domain walls. The virgin 180° domain walls exhibit smooth lines of transition between up and down domains, while the geometries of the clusters are similar to the previously observed etch grooves [17].

Bipolar loading yields a significant reduction of the polarization amplitude not encountered after unipolar electrical loading and much less after mixed electromechanical loading (electric unipolar and mechanically compressive, 180° out of phase). No etch grooves are observed for unipolar loading and very few in the latter case. Thus, bipolar loading predominantly induces the etch grooves. In order to grow during cyclic loading, the clusters need a sufficient flux of incoming point defects. No loss of oxygen occurs due to fatigue in bulk ferroelectrics [23]. Nevertheless, oxygen vacancies are commonly assumed the most mobile point defects in the structure [24]. Dawber and Scott assumed the clustering of oxygen vacancies the relevant fatigue mechanism and based a cluster growth model on this assumption [16]. Cluster growth here is also considered to be provided by

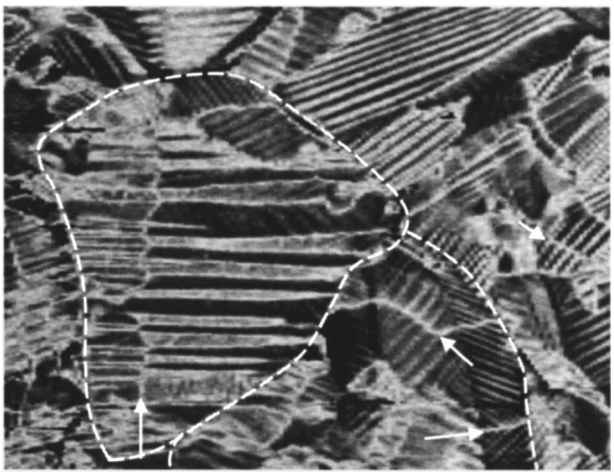

FIG. 3. Atomic force microscopic image of a cluster in a grain of lead-zirconate-titanate. The arrows indicate cluster locations appearing as bright uneven lines (image width 17 μm).

point defects introduced during sample processing, but irrespective of polarity and whether they are dopant ions, vacancies, or localized electronic states. The charge current density j_e in ionic solids is generally given by [25]

$$j_e = 2\rho ezbP \sinh\left(\frac{Eeb}{2kT}\right) =: \rho\gamma, \qquad P = \xi \frac{kT}{h} \exp\left(\frac{G}{kT}\right), \tag{1}$$

ρ is the volume density of charged defects, ze their charge, b the hopping distance between two sites (lattice constant), P the probability of an ion jump, including the attempt frequency $\xi \frac{kT}{h}$, E the electric field, k Boltzmann's constant, ξ a coordination parameter of the lattice site, h Planck's constant, G the Gibb's free energy, and γ a dummy. The externally applied electric field yields an ion flux which is several orders of magnitude too low for explaining the observed growth rate of the clusters during cycling at room temperature. Thermal diffusion yields even lower rates. The ionic flux is thus driven by local fields much higher than the external field ($E_a = 2$ kV/mm). Such a field can be provided only by the local depolarizing field [6,26] ($E_{\text{depol}} = 100$ kV/mm, if no screening exists). The global charge mismatch is compensated in the metallic electrodes, but high local fluctuations occur during bipolar switching, particularly in a polycrystalline material. Here, the vector components of polarization perpendicular to the external field direction cannot be screened in the electrodes. As j_e in Eq. (1) exponentially depends on the electric field, the differences in ionic flux become enormous. Figure 4 displays a state around an already existing cluster during bipolar switching. The stable induced needle domain is embedded in a larger domain of opposite polarity, which has not yet reversed. Before remote domains of the same polarity as the needle reach the cluster, i.e., just before the macroscopic coercive field is reached, the depolarizing field can almost fully develop underneath the cluster during a brief fraction of the applied field cycle. A large ion flux is driven towards the cluster. Colla *et al.* showed in thin films that the fatigue rate becomes enormous, if the samples are held just beneath the coercive field for an extended period of time before full switching, but they were not able to give a satisfying explanation [27].

In order to support this mechanism, a uniaxial model of cluster growth is presented. The total ion flux into the cluster is constituted by two contributions. The first is the ionic flux according to Eq. (1) and thus different from the linear assumption by Dawber and Scott [16]; the second is due to the capturing of all ions in a finite volume of height $\alpha \cdot r$ beneath the cluster of radius r due to the geometrical growth of the cluster, α being a proportionality constant. A certain fraction ζ of the entire bipolar sinusoidal cycle yields voltages just beneath the coercive field. A primary concentration ρ_0 of isolated defects is given. A finite volume $g \gg r^3$, being, e.g., one grain or a representative volume, provides the source of point defects for the assumed single cluster in this volume. It determines a maximum relative concentration of defects $\rho_{\text{relative}} < 3b/8g \approx 10^{-4}$ in the numerical case beneath. During cluster growth, the concentration of isolated defects decreases. A simple rate equation yields the implicit dependence of agglomerated ions N_A on the initial number of defect ions N and the cycle number n:

$$n \approx -\frac{1}{\gamma b^2 \rho_0} \ln\frac{N - N_A}{N_A} + \frac{3\alpha b}{2\sqrt{\pi}\gamma} N \ln\frac{\sqrt{N} - \sqrt{N_A}}{\sqrt{N} + \sqrt{N_A}} - 2\frac{\alpha b}{\sqrt{\pi}\gamma}\sqrt{N_A}. \tag{2}$$

Figure 5 displays the growth of point defect clusters [Eq. (2), $\xi = 1$, $\alpha = 1$, $T = 350$ K, $\zeta = 0.1$, $g = 5$ μm, $G = 1$ eV, $\rho_0 b^3 = 10^{-4}$, $b = 0.4$ nm]. In experiment, the most significant reduction of polarization occurs at around 10^6 cycles [17]. Field values around the depolarizing field are necessary to match this cycle number exceeding the external field (2 kV/mm) by more than an order of magnitude. The unscreening [26] of the depolarizing field is thus a necessary consequence for the fatigue mechanism. This effect cannot occur in unipolar scenarios, because all domains remain in a more or less compensated environment. Different from previous assumptions on the relation between blocked domains and

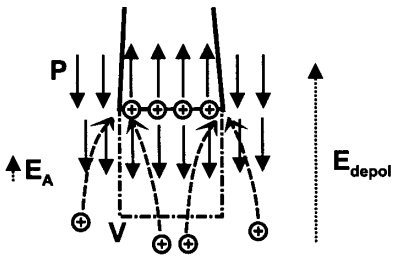

FIG. 4. Illustration of the electric fields (dotted lines) around a charged point defect cluster before polarization (P) switching of the embedding larger domain just beneath the macroscopic coercive field. A volume of point defect depletion and the migration paths (dashed lines) of defects are sketched.

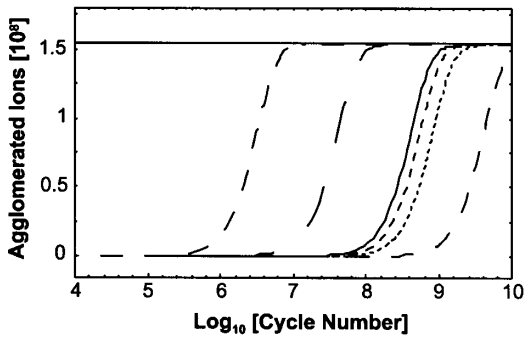

FIG. 5. Field dependence of agglomeration [Eq. (2)] for the local fields (left to right): 200, 20, 2, 1.5, 1, and 0.2 kV/mm

lost polarization [16], it is here assumed that the number of blocked domains is proportional to the number of clusters exceeding a particular critical size on the order of the width of a domain.

We modeled other microscopic geometries and cluster growth conditions each yielding term of the form of the first two terms in Eq. (2) and curves similar to Fig. 5. In any case, the agglomeration rates provided by the external electric field turn out to be more than an order of magnitude too low. All models saturate when all isolated point defects have been incorporated into the clusters.

In some experiments, the agglomeration rate becomes slower about halfway up the cluster growth curve [17,28]. Microscopically, this corresponds to needle domains reaching, e.g., a grain boundary. As ionic diffusion may be limited across internal boundaries, the influx is no longer determined by the fields alone, but also by transverse diffusion rendering the agglomeration process much slower.

In an early study by Kudzin, the formation of needle domains along [001] was optically observed in $BaTiO_3$ single crystals, but the identification of planar point defect clusters at the origin of the needle domains in the interior of the crystal as well as any mechanism for the formation of such clusters remained unexplained [29].

Point defect clustering was proven to occur only if the flux of charged point defects into such clusters is dramatically enhanced with respect to thermal diffusion or the defect flux driven by external fields. Only a scenario where the depolarizing field of a ferroelectric becomes temporarily unscreened locally can explain the dramatically increased ion flux at room temperature by several orders of magnitude. The so far completely puzzling difference between unipolar and bipolar fatigue becomes evident considering this mechanism.

The support by the Deutsche Forschungsgemeinschaft (Lu729/4 and Ar666/66), the critical review of the paper by Walter Arnold, and discussions with Jürgen Rödel, Cyril Verdier, and Jürgen Nuffer are greatly acknowledged. The authors are grateful to Alexandre Pedrosa Goncalves for skillfully taking a large number of AFM images.

[1] J. F. Scott, *Ferroelectric Memories* (Springer-Verlag, Berlin, 2000).
[2] K. Uchino, *Piezoelectric Actuators and Ultrasonic Motors* (Kluwer Academic, Boston, 1997).
[3] B. Jaffe, W. R. Cook, Jr., and H. Jaffe, *Piezoelectric Ceramics* (Academic, Marietta, OH, 1971).
[4] C. A. Randall, N. Kim, J. P. Kucera, W. Cao, and T. R. Shrout, J. Am. Ceram. Soc. **81**, 677 (1998).
[5] G. Arlt, J. Mater. Sci. **25**, 2655 (1990).
[6] M. E. Lines and A. M. Glass, *Principles and Applications of Ferroelectrics and Related Materials* (Clarendon, Oxford, 1977).
[7] D. Lupascu, V. Shur, and A. Shur, Appl. Phys. Lett. **81**, 2359 (2002).
[8] J. C. Grenier, M. Pouchard, and P. Hagenmuller, Struct. Bond. **47**, 2 (1981).
[9] T. Suzuki, M. Ueno, Y. Nishi, and M. Fujimoto, J. Am. Ceram. Soc. **84**, 200 (2001).
[10] C. H. Park and D. J. Chadi, Phys. Rev. B **57**, R13961 (1998).
[11] C. Brennan, Ferroelectrics **150**, 199 (1993).
[12] P. Grenier, S. Jandl, M. Blouin, and L. A. Boatner, Ferroelectrics **137**, 105 (1992).
[13] J. F. Scott and M. Dawber, Appl. Phys. Lett. **76**, 3801 (2000).
[14] J. F. Scott and M. Dawber, J. Phys. IV (France) **11**, Pr11-9 (2001).
[15] A. I. Becerro, C. McCammon, F. Langenhorst, F. Seifert, and R. Angel, Phase Transit. **69**, 133 (1999).
[16] M. Dawber and J. Scott, Appl. Phys. Lett. **76**, 1060 (2000).
[17] J. Nuffer, D. C. Lupascu, and J. Rödel, Acta Mater. **48**, 3783 (2000).
[18] K. Franke, J. Besold, W. Haessler, and C. Seegebarth, Surf. Sci. Lett. **302**, L283 (1994).
[19] L. M. Eng, H.-J. Güntherod, G. A. Schneider, U. Köpke, and J. Muñoz-Saldana, Appl. Phys. Lett. **74**, 233 (1999).
[20] U. Rabe, M. Kopycinska, S. Hirsekorn, and W. Arnold, Ultrasonics **40**, 49 (2002).
[21] A. Gruverman, O. Kolosov, J. Hatano, K. Takahashi, and H. Tokumoto, J. Vac. Sci. Technol. B **13**, 1095 (1995).
[22] G. Arlt and P. Sasko, J. Appl. Phys. **51**, 4956 (1980).
[23] J. Nuffer, M. Schröder, D. C. Lupascu, and J. Rödel, Appl. Phys. Lett. **79**, 3675 (2001).
[24] I. Denk, W. Münch, and J. Maier, J. Am. Ceram. Soc. **78**, 3265 (1995).
[25] L. L. Hench and J. K. West, *Principles of Electronic Ceramics* (Wiley, New York, 1990).
[26] V. Y. Shur, V. V. Letuchev, and Y. A. Popov, Sov. Phys. Solid State **24**, 1618 (1982).
[27] E. L. Colla, A. K. Tagantsev, D. V. Taylor, and A. L. Kholkin, Integr. Ferroelectrics **18**, 19 (1997).
[28] C. Pawlaczyk, A. K. Tagantsev, K. Brooks, I. M. Reaney, R. Klissurska, and N. Setter, Integr. Ferroelectrics **8**, 293 (1995).
[29] A. Y. Kudzin, T. V. Panchenko, and S. P. Yudin, Sov. Phys. Solid State **16**, 1589 (1975).